Extrasolar planet detection through spatially resolved observations

Meshkat, T.R.

Chapter 6

Searching for gas giant planets on Solar System scales - A NACO/APP L'-band survey of A- and F-type Main Sequence stars

We report the results of a direct imaging survey of A- and F-type main sequence stars searching for giant planets. A/F stars are often the targets of surveys, as they are thought to have more massive giant planets relative to solar-type stars. However, most imaging is only sensitive to orbital separations >30 AU, where it has been demonstrated that giant planets are rare. In this survey, we take advantage of the high-contrast capabilities of the Apodizing Phase Plate coronagraph on NACO at the Very Large Telescope. Combined with optimized principal component analysis post-processing, we are sensitive to planetary-mass companions (2 to 12 $M_{\rm Jup}$) at Solar System scales ($\leq$30 AU). We obtained data on 13 stars in L'-band and detected one new companion as part of this survey: an M6.0 $\pm$ 0.5 dwarf companion around HD 984. We re-detect low-mass companions around HD 12894 and HD 20385, both reported shortly after the completion of this survey. We use Monte Carlo simulations to determine new constraints on the low-mass (<80 $M_{\rm Jup}$) companion frequency, as a function of mass and separation. Assuming solar-type planet mass and separation distributions, normalized to the planet frequency appropriate for A-stars, and the observed companion mass-ratio distribution for stellar companions extrapolated to planetary masses, we derive a truncation radius for the planetary mass companion surface density of <80 AU at 95% confidence. Finally, we compare the performance of the APP with direct imaging for four of our targets and discuss when the sensitivity is improved.

T. Meshkat, M. A. Kenworthy, M. Reggiani, S. P. Quanz, E. E. Mamajek, M. R. Meyer

Submitted to *Monthly Notices of the Royal Astronomical Society*

6.1 Introduction

Stellar properties are an important metric in the search for planets, as they guide the target selection for detection surveys. In particular, stellar mass and metallicity are significant quantities in determining both the formation and evolution of stars and planets (Johnson et al. 2010). Several radial velocity (RV) studies have shown that the giant planet frequency increases with stellar metallicity (Santos et al. 2004; Fischer & Valenti 2005). The giant planet population as a function of stellar mass, however, is not consistent between different planet detection techniques (Quanz et al. 2012; Clanton & Gaudi 2014; Vigan et al. 2012). While progress has been made in linking the RV and microlensing populations (Clanton & Gaudi 2014), this is a challenging problem involving the synthesis of different biases and parameter spaces covered by all the detection techniques.

Hot, gas giant planets ($> 1\,M_{\rm Jup}$) are the only directly imaged planets thus far, due to their increased self-luminous thermal emission and decreased contrast at infrared wavelengths with the star. Planet populations derived from RV surveys are often extrapolated to larger orbital separations to analyze the frequency of giant planets in direct imaging surveys (e.g. Lafrenière et al. 2007; Biller et al. 2013).

Planet formation scenarios (Alibert et al. 2011) and simulations extrapolating RV planet populations (Crepp & Johnson 2011; Johnson et al. 2007) suggest that massive stars($>1.3M_{\odot}$) are the most favorable targets for directly imaging planets, since they have proportionally more material to form giant planets. Indeed many directly imaged planetary mass companions have been found around A or F stars: HR8799 bcde (Marois et al. 2008, 2010), β Pic b (Lagrange et al. 2009, 2010), HD 95086 b (Rameau et al. 2013b,c), HD 106906 b (Bailey et al. 2014). The detection of the HR8799 planets was the result of the Vigan et al. (2012) International Deep Planet Survey. Most surveys, however, have yielded null results (Desidera et al. 2015; Chauvin et al. 2015; Janson et al. 2013; Rameau et al. 2013a; Biller et al. 2013; Chauvin et al. 2010; Heinze et al. 2010; Lafrenière et al. 2007; Kasper et al. 2007). These null results are likely due to the lack of contrast at small orbital separations. Typical detection limits for these surveys are 5-20 $M_{\rm Jup}$ for > 30 AU. Planets are rare at large orbital separations (Chauvin et al. 2010; Lafrenière et al. 2007; Nielsen & Close 2010) but at Solar System scales (≤ 30 AU), stars are largely unexplored.

The main limitations for direct imaging are stellar "speckles" which can appear brighter than a companion (Hinkley et al. 2009). Coronagraphs are used in order to reach smaller angular separations around stars. They reduce the diffraction due to scattered stellar light in the telescope optics but at a cost of reduced throughput. The Apodizing Phase Plate (APP; Kenworthy et al. 2010; Quanz et al. 2010, 2013) coronagraph suppresses the diffraction in a 180° wedge around a star, increasing the chances of detecting a very close-in companion. Several studies have demonstrated the APP's capability of reaching ≤ 30 AU (Meshkat et al. 2015; Kenworthy et al. 2013; Quanz et al. 2011).

We aim to probe down to Solar System scales (≤ 30 AU) around 13 A- and F-type main sequence stars in order to detect giant planets as well as set constraints

on the planet frequency. We use the APP coronagraph on NACO at the Very Large Telescope (VLT), the L'-band filter, and optimized Principal Component Analysis (PCA) to achieve deep sensitivity limits (2 to 10 $M_{\rm Jup}$ at ≤ 30 AU).

In Section 6.2 we describe our target selection process, the coronagraphic observations, our data reduction method and how we determine the sensitivity of our data. In Section 6.3 we discuss the sensitivity achieved, our new detection of an M6.0 ± 0.5 dwarf companion to HD 984, and our re-detection of companions to HD 12894 and HD 20385. We run Monte Carlo simulations to determine the probability distribution of our results, in order to compare different planet population models for A- and solar-type stars. In Section 6.4 we compare our results with other surveys searching for low-mass companions and discuss the performance of the APP coronagraph. Our conclusions are in Section 6.5.

6.2 Observations and Data Reduction

Our sample was carefully selected to derive the best possible constraints on the frequency of giant exoplanets on Solar System scales: nearby, young, and massive main sequence stars. Young planets are still warm from their contraction (Spiegel & Burrows 2012). By converting gravitational energy into luminosity, they are bright in the infrared. However, determining the age of a main-sequence star can be extremely challenging. One way to deal with this difficulty is to only select targets which are members of nearby associations with well established ages. If they are all bona-fide members of the group, we can assume the stars are of a similar age. Except for one[1], our targets are all members of nearby young moving groups or associations: β Pic Moving Group (23 ± 3 Myr; Mamajek & Bell 2014), Tuc-Hor Association (40 Myr; Kraus et al. 2014), AB Dor Association (125 ± 15 Myr; Barenfeld et al. 2013). Nearby stars allow us to search for companions at smaller physical separations. We aim to reach planet sensitivity on Solar System scales, where we expect more planets to reside (Chauvin et al. 2010; Lafrenière et al. 2007; Nielsen & Close 2010). Thus, we have selected only stars which are less than 66 pc away.

At the time of selection, most[2] of the targets were known to be single stars (Mason et al. 2011; Pourbaix et al. 2009) and not in the denser nucleus of their association. However, shortly after our survey was completed, a companion was discovered around one of our targets, HD 12894, by Biller et al. (2013) and Rameau et al. (2013a). Another target, HD 20385, was found to have a companion shortly after our data were acquired (Hartkopf et al. 2012).

6.2.1 Observations at the VLT

Data were obtained for 13 targets from 2011 to 2013 (088.C-0806(B), 089.C-0617(A) PI: Sascha Quanz) at the Very Large Telescope (VLT)/UT4 with NACO

[1] At the time of our observations, HD 984, was believed to be a 30 Myr member of Columba association. Based on our detection of a low-mass stellar companion to HD 984 and independent isochrone fitting, we estimate the age of HD 984 to be ~2 Gyr (Meshkat et al. *submitted*).

[2] HD 20385 was known to have a wide binary 12" away.

Target	Mass ($M_\odot$)	L' mag	Spectral type	Distance (pc)	Age (Myr)
HD 203	1.40	5.2	F3V	39.4 ± 0.6	23
HD 12894	1.39	5.5	F4V	47.8 ± 1.0	40
HD 25457	1.21	4.3	F6V	18.8 ± 0.1	125
HD 35114	1.16	6.2	F6V	8.3 ± 0.9	40
HD 20385	1.13	6.4	F6V	49.2 ± 1.5	40
HD 102647	1.9	1.9	A3Va	11.0 ± 0.1	40
HD 984	1.18	6.0	F7V	47.1 ± 1.4	2000
HD 13246	1.18	6.2	F7V	44.2 ± 0.9	40
HD 40216	1.24	6.2	F7V	54.4 ± 1.3	40
HD 30051	1.38	6.0	F2/3IV/V	63.6 ± 4.2	40
HD 25953	1.16	6.6	F5	55.2 ± 2.9	125
HD 96819	2.09	5.2	A1V	55.6 ± 1.7	23
HD 123058	1.30	6.7	F4V	64.1 ± 3.5	40

Distances are extracted from parallaxes in the Hipparcos catalog (van Leeuwen 2007). The L'-band mag is converted from K-band mag in the 2MASS survey (Cutri et al. 2003) to using Cox (2000). The masses are from Casagrande et al. (2011) and Chen et al. (2014). All ages are taken from Mamajek & Bell (2014); Kraus et al. (2014); Luhman et al. (2005); Barenfeld et al. (2013) except for HD 984 which we compute in Meshkat et al. *submitted*. The bottom six targets were only observed in one APP hemisphere.

Table 6.1 Overview of stellar values used for each target.

(Lenzen et al. 2003; Rousset et al. 2003) and the APP coronagraph (Kenworthy et al. 2010). The variation in the observing time for each target depends on the observing conditions on the night; if the observing conditions fell below a threshold during the night, the data acquisition was cancelled. Data were obtained with the L27 camera, in the L'-band filter ($\lambda = 3.80\mu$m and $\Delta\lambda = 0.62\mu$m) and the NB 4.05 filter ($\lambda = 4.051\mu$m and $\Delta\lambda = 0.02\mu$m) depending on the star's L'-band magnitude. The visible wavefront sensor was used with each target star as its own natural guide star. We observed in pupil tracking mode to perform Angular Differential Imaging (ADI; Marois et al. 2006). We intentionally saturated the point spread function (PSF) core (on average out to ~0.″08) to increase the signal-to-noise (S/N) from potential companions in each exposure. Unsaturated data were also obtained to calibrate photometry relative to the central star.

The APP generates a dark D-shaped wedge on one half of a target. Excess scattered light is increased on the other side of the target, which is not used in the data analysis. Two datasets were obtained with different initial position angles (P.A.) for full 360° coverage around the target star. Data were obtained in cube mode. Table 6.1 lists the stellar properties for each of our targets. Table 6.2 lists the observing conditions for all the data obtained. 13 targets were observed in at least one APP hemisphere.

6.2.2 Data Reduction

A dither pattern on the detector was used to subtract sky background and detector systematics from the raw data, as detailed in Kenworthy et al. (2013). Subtracted data cubes are centroided and averaged over. The two APP hemispheres obtained for each target must be processed separately, since they were observed on different nights and thus have different speckle noise patterns. Optimized PCA was run on both of the APP hemispheres independently for each target, following Meshkat

Target	Observation dates UT (Hem 1, Hem 2)	Number of data cubes	Total integration time (s)	On-sky rotation (°)	Average DIMM seeing (")
HD 203	2011 Oct 12, 2011 Nov 07	154, 64	4605.3, 3480.75	46.65, 60.43	0.90,1.19
HD 12894	2011 Dec 10, 2011 Dec 24	65, 55	3333, 2828	31.97, 27.92	0.78,1.23
HD 25457	2011 Dec 11, 2011 Dec 21	71, 65	2606.4, 2389.2	28.63, 25.92	1.44,0.65
HD 35114	2011 Dec 13, 2012 Jan 02	35, 35	1818, 1818	31.98, 28.20	0.75,1.02
HD 20385	2011 Dec 21, 2012 Jan 08	47, 35	2424, 1818	30.54, 24.61	1.82,1.25
HD 102647	2012 Jun 01, 2013 Apr 26	47, 56	2839.2, 3371.6	20.34, 24.71	1.61, 0.76
HD 984	2012 Jul 18, 2012 Jul 20	59, 65	3267, 3593.7	47.41,42.46	0.65, 0.86
HD 13246	2011 Dec 07, –	107, –	5454, –	45.43, –	0.99, –
HD 40216	2012 Jan 03, –	11, –	606, –	11.74, –	0.88, –
HD 30051	2012 Jan 07, –	56, –	2878.5, –	2.7, –	1.68, –
HD 25953	2012 Jan 13, –	79, –	4040, –	42.76, –	0.77, –
HD 96819	2012 May 02, –	49, –	2835, –	105.46, –	0.64, –
HD 123058	2012 May 21, –	62, –	3811.5, –	29.44, –	0.77, –

Data are in chronological order based on first Hemisphere observed. The last six targets were only observed in one APP hemisphere. Targets are listed in the same order as Table 6.1.

Table 6.2 Observing Log for NACO/VLT 088.C-0806(B) and 089.C-0617(A)

et al. (2014). This involves creating a linear combination of principal components (PCs) from the data itself in order to model and subtract away the stellar diffraction. Only the 180° D-shaped dark hemisphere was used in the PCA analysis. We fixed the number of PCs at approximately 10% the number of input frames, as this yields the optimal PSF subtraction close ($< 1\farcs0$) to the star. We searched for point sources using this method for all 13 of our targets, despite not having full 360° coverage for 6 of them.

We injected fake planets into our data (before PCA processing) in order to determine the 5σ sensitivity limit for each target. Unsaturated data of the star was used to inject the fake planets. We scaled the unsaturated data to the same exposure as the saturated data. The star was added to the data with a contrast of 5 to 12 mag in steps of 1 mag and from $0\farcs18$ to $1\farcs36$ in steps of 0.13. The outer radius limit was chosen because the field-of-view (FOV) of the APP is limited to only the upper quarter of the detector (Kenworthy et al. 2010). The planet injected data was processed with PCA, de-rotated, and averaged over for the final image with North facing up.

The final image was smoothed by a λ/D aperture, in order to remove features which are not the expected planet size or shape (Amara & Quanz 2012; Bailey et al. 2013). We define the S/N of the injected planet to be the value of a single pixel at the location of the planet divided by the root mean square (rms) of a ring around the star at the angular separation of the planet, excluding the planet itself. Only the statistically independent pixels (one smoothing kernel apart) were used

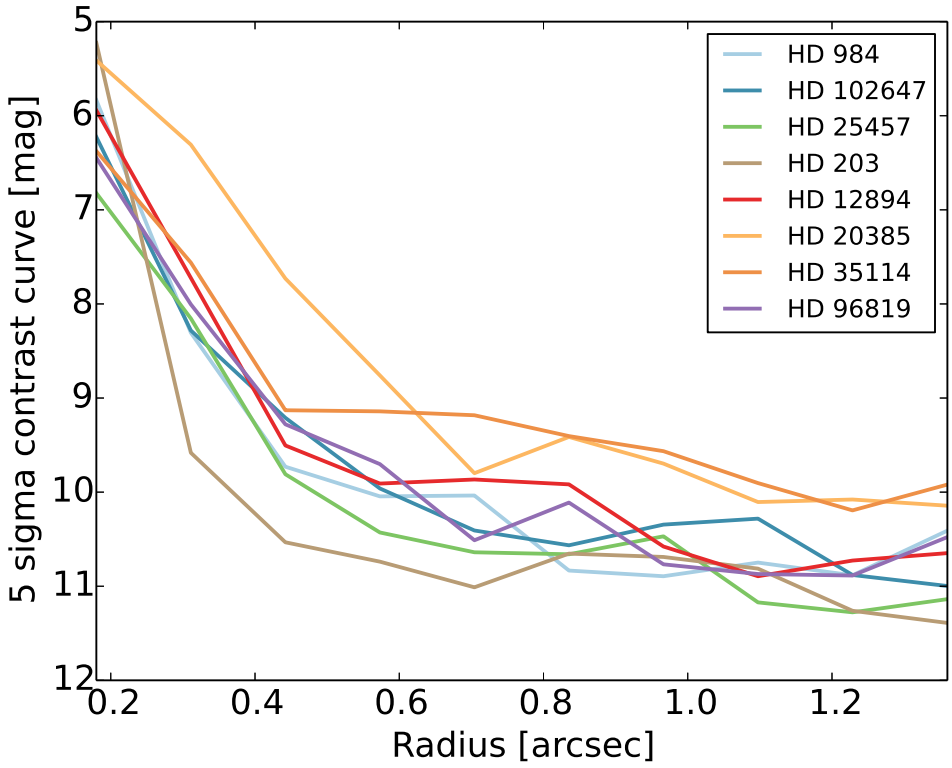

Figure 6.1 5σ contrast curves for the targets with full 360° APP coverage around the star and one target, HD 96819, with nearly 360° coverage.

to compute the rms. Figure 6.1 shows the 5σ contrast curves for all 7 targets with two APP hemispheres and one target (HD 96819) with nearly full sky coverage in one APP hemisphere[3]. For targets with two APP hemispheres, fake planets were added at a fixed P.A. in each hemisphere. The average S/N of the injected fake planets in each hemisphere is used (at the same separation). In the overlapping region between the two hemispheres, the number of frames varies slightly. However, since these regions are small and the number of frames never varies by more than 20%, the impact on the contrast curves is small.

On average, we achieved a contrast of 9 mag at 0.″4 and 10 to 11 mag at > 0.″6. The decreased sensitivity at < 0.″7 around HD 20385 is an outlier compared to the other targets. One possible explanation is the extremely bright companion detected at ∼ 0.″8 (discussed in Section 6.3.2), which affects the PCA component determination.

We used the COND evolutionary tracks (Baraffe et al. 2003) to convert the contrast curves to planet mass detection limits (Figure 6.2). For all but one of

[3]HD 96819 has on sky rotation of 105.°46. Since we are in ADI mode, the 180° APP "dark hole" region rotates on the sky and only a ∼ 74.°9 wedge is missing.

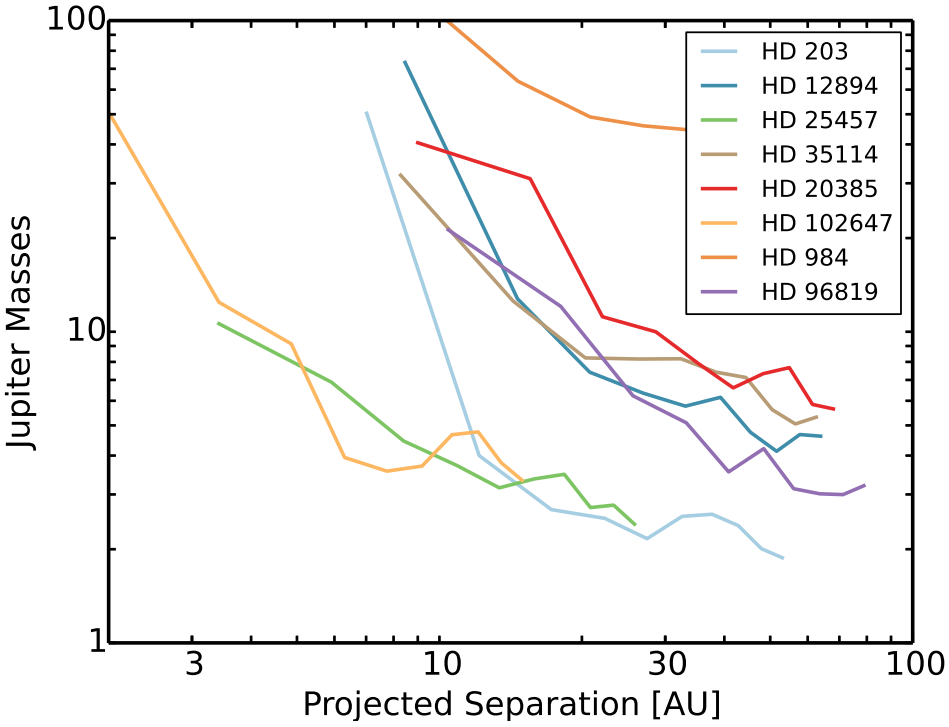

Figure 6.2 Detection limits in Jupiter masses versus projected separation in AU for all targets with full APP coverage (and HD 96819). We are sensitive to planet mass companions ($< 12 M_{\rm Jup}$) for all of our targets, except HD 984 which we demonstrate is much older than previously suggested (Meshkat et al. *submitted*). HD 102647 is more sensitive at smaller projected separation because it is much closer than the rest of the targets (11 pc). We do not plot the sensitivity beyond 1.″5 for each target, due to the limited FOV of the APP.

Target	Date	Separation (arcsec)	P.A. (deg)	$\Delta L'$ (mag))	Mass ($M_\odot$)
HD12894 B	2011 Nov 24	0.31 ± 0.01	240.24 ± 1.36	2.89 ± 0.14	0.49 ± 0.04
HD20385 B	2011 Dec 21	0.87 ± 0.01	118.67 ± 0.7	2.52 ± 0.10	0.43 ± 0.03
HD984 B	2012 July 18	0.19 ± 0.02	108.9 ± 3.1	6.0 ± 0.2	0.11 ± 0.01

Table 6.3 Companion properties of our targets.

our targets[4], we were sensitive to planetary mass objects ($< 12\,M_{\rm Jup}$) at different projected separations, depending on the target distance. The outer radius for the sensitivity curves is based on the limited FOV of the APP (Kenworthy et al. 2010). Thus, while the sensitivity curves appear to flatten out, we cannot extend these curves beyond 1.″5 since we were not sensitive completely around the star.

6.3 Results

We detect one new M6.0 ± 0.5 dwarf companion to HD 984, and re-detect companions to HD 12894 and HD 20385. To estimate the astrometry, we first determine the centroid of the three companions. In this way, we verify that our star was well centered in our data. Since the APP has an asymmetric PSF, this step is crucial. We then injected fake negative companions at the location of the companion to determine the photometry and astrometry with error bars. We also varied the flux of the fake negative companions to cancel out the companion flux, which in some cases varies up to 20% due to atmospheric fluctuations.

We iteratively converged on the P.A., angular separation, and Δ magnitude by varying the position and contrast and taking a χ^2 minimization over the λ/D aperture at the location of the companion. For the very bright companions to HD 12894 and HD 20385, we determined the photometry and astrometry from ADI alone rather than PCA. Minor variations in the brightness and position of the companion in each frame can lead to "striping" in the final PCA processed image. This striping occurs when PCA fits the remaining flux around of the companion after the fake companion is subtracted, since we never perfectly subtract the companion in individual frames due to seeing variability. Table 6.3 lists the properties of the companions we detect based on our APP data. The error on the P.A. includes uncertainties from true North orientation, based on direct imaging observations ($\sim 0.5°$, Rameau et al. 2013a).

6.3.1 HD 12894

Rameau et al. (2013a) and Biller et al. (2013) reported the discovery of HD 12894 B. Rameau et al. (2013a) detected a $\Delta L' = 2.7 \pm 0.1$ mag point source 14 AU from the star. They concluded that it was likely bound to the star, based on a non-detection in 1999 2MASS data, because a background source would be detected due to proper motion of HD 12894. Based on the contrast and an age of 30 Myr, they concluded that the companion was a $0.8 M_\odot$ K6 star. Biller et al. (2013)

[4]We were not sensitive to planet masses around HD 984, since it is much older than previously reported (Meshkat et al. *submitted*).

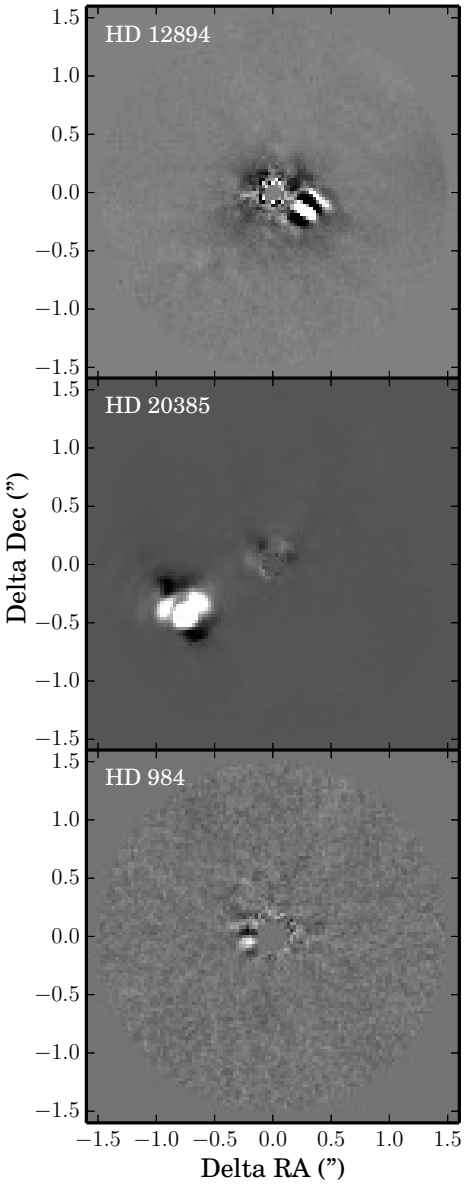

Figure 6.3 Top: HD 12894 ADI processed image, with the companion at 0.″31. Middle: HD 20385 ADI processed image, with the companion at 0.″87. The shape of the companion PSF is due to the APP PSF. Bottom: HD 984 PCA processed image with the companion 0.″192 from star.

concluded it was a co-moving $0.46 \pm 0.08\ M_{\odot}$ companion 15.7 ± 1.0 AU away from its star, based on contrast of $\Delta H = 3.0$ mag. The discovery was made with the VLT/NACO instrument in L'-band as well as the NICI instrument on Gemini South in H-band, respectively.

At the time our data were acquired, the companion was not known. We detect the companion with a $\Delta L' = 2.89 \pm 0.14$ mag at a PA of $240.24 \pm 1.^{\circ}27$ and separation of $0.''31 \pm 0.''01$. This corresponds to a projected separation of 14.8 ± 0.8 AU, with d=47.8 ± 1.0 pc for the distance to the star (van Leeuwen 2007). Figure 6.3 shows the ADI processed image of the companion. Using the COND evolutionary models (Baraffe et al. 2003) and the age of the star (40 Myr: Kraus et al. 2014), we estimate the mass of the companion is $0.49 \pm 0.04\ M_{\odot}$. Our analysis of this companion is consistent with Biller et al. (2013).

6.3.2 HD 20385

At the time we proposed to observe this target, it was a known wide binary, with a companion TOK 78 B 12" away. Hartkopf et al. (2012) reported the discovery of a new, close companion around HD 20385 at $0.''88$, ΔI =3.5 mag, Δy = 5.2 mag. They estimated the companion has a period of 200 years. Due to its variable radial velocity, they suggested the companion could be two unresolved companions.

We detect the companion in our data at $0.''87 \pm 0.''01$ with a P.A. of $118.^{\circ}67 \pm 0.^{\circ}49$ and contrast of $\Delta L' = 2.52 \pm 0.10$ mag. Using the stellar distance of 49.2 ± 1.5 pc (van Leeuwen 2007), this companion is at a projected separation of 42.8 ± 1.8 AU. Figure 6.3 shows the ADI processed image of the companion to HD 20385. The companion's PSF clearly shows the APP PSF structure, with the bright lobes smeared due to the rotation on the sky. The age of the system is 40 Myr based on membership in the Tuc-Hor Association (Kraus et al. 2014). Using COND models (Baraffe et al. 2003), we estimate the companion to have a mass of $0.33 \pm 0.03\ M_{\odot}$.

6.3.3 HD 984

As reported in Meshkat et al. (*submitted*), we detected a companion around HD 984 in our APP data, as well as in archival direct imaging data. Figure 6.3 shows our PCA reduced image with 20 PCs. We confirmed the companion is co-moving with HD 984 and determined that is an M6.0 ± 0.5 dwarf based on SINFONI integral field spectroscopy (see Table 6.3).

6.3.4 Monte Carlo Simulations

We ran 10000 Monte Carlo simulations of the target stars in order to determine the probability distribution of detecting substellar companions in our data assuming power-law slopes for the mass and semi-major axis distributions, for both planets and brown dwarfs (BDs), following Reggiani et al. *submitted*. For the BD distribution, we adopted the stellar companion mass ratio distribution (CMRD) from Reggiani & Meyer (2013) and a log-normal separation distribution (De Rosa et al. 2014). We included all of our targets in these simulations, including those with

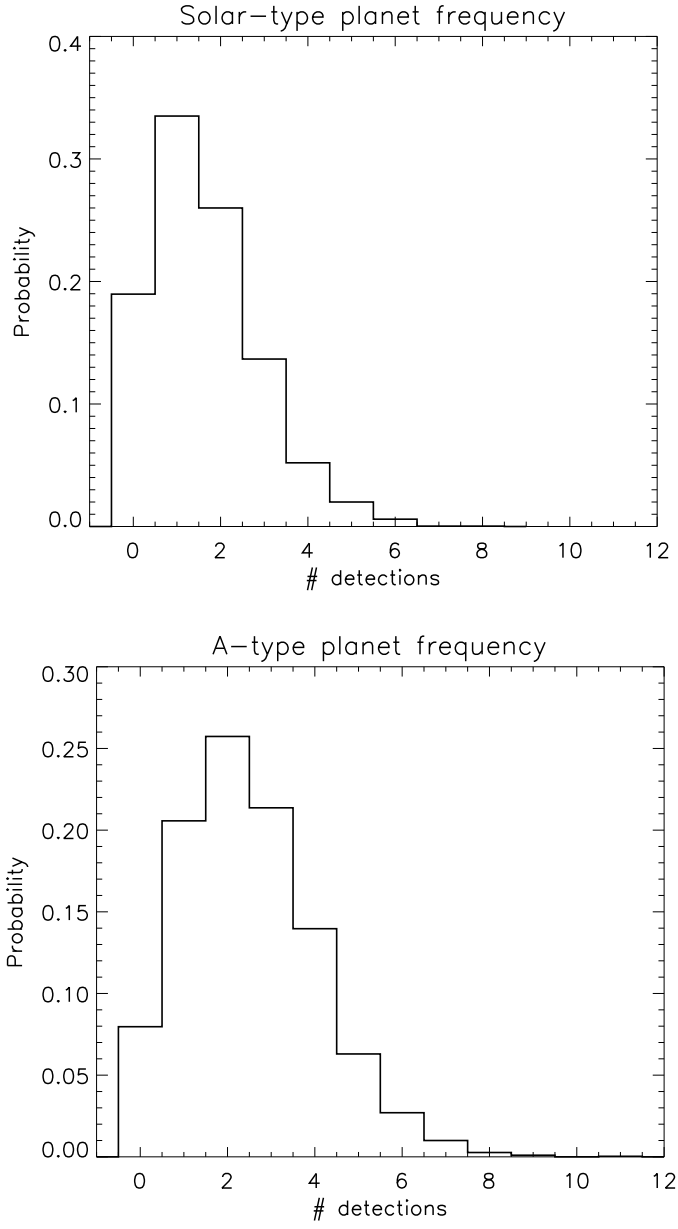

Figure 6.4 Detection probability distributions for our survey, assuming an outer-radius cutoff of 80 AU for the planet separation distributions (Reggiani et al., *submitted*). We run the simulations for both solar-type stars and A-stars. With our null result, we rule out the A-star frequency beyond a cutoff of 100 AU at the 95% confidence level. (Top: solar-type stars, Bottom: A-type stars).

only one APP hemisphere coverage. In order to account for the targets without full sky coverage in our simulations, we multiplied the overall planet frequency per target by the fraction of sky coverage achieved.

For the planets, we adopted two different model distributions. The first one assumes the planet frequency, mass and separation distributions measured by RV surveys for solar-type stars, and extrapolated at larger separations (Heinze et al. 2010, based on Cumming et al. 2008). According to Cumming et al. (2008), the planet mass and semi-major axis distributions are modeled with power laws of index α=-1.31 and β=-0.61 ($dN \sim M^{-1.31}dM$ and $dN \sim a^{-0.61}da$). This results in a planet frequency of f=0.0329 for planets in the range 1-13 $M_{\rm Jup}$ and 0.3-2.5 AU. The second model, more appropriate for A-type primaries, consists of the same planet mass and separation distribution measured for Sun-like stars, but adopts the values corresponding to the median sensitivity achieved in the RV data presented in Bowler et al. (2010) and Johnson et al. (2010) (f=11 ± 2% for planets in the ranges 0.5-14 $M_{\rm Jup}$ and 0.1-3.0 AU).

For both planets and BDs, we assume a random distribution of inclinations and the eccentricity distribution given by Jurić & Tremaine (2008). In each simulation, we assigned each target a number of planets and BDs from a Poisson distribution, according to the average number of planets and BDs per star, calculated from the aforementioned distributions. As this is given by the BD and planet mass and separation probability distributions, it is different in the two models for the planet population. We also varied the outer radius cutoff: 20, 30, 80, and 100 AU. The introduction of an upper limit for the planet separation distribution has been suggested by the results of previous direct imaging surveys (Chauvin et al. 2010; Vigan et al. 2012).

If a target turns out to have one or more companions in the simulation, we assigned each companion a mass and the orbital parameters (semi-major axis, eccentricity, inclination) randomly drawn from the assumed distributions. The mass is converted into apparent magnitude, given the distance and age of the star and assuming the same family of evolutionary models as in Section 6.2.2 (COND Baraffe et al. 2003). The semi-major axis was converted into a projected separation, given the eccentricity and inclination and taking into account the time spent on the orbit. If the combination of brightness and separation lies above the contrast curve (Figure 6.1), then the companion is detectable. Thus, at the end of every simulation, we know how many companions are created and how many are detected. After 10000 simulations, we determined the average detection probability for our A and F main sequence star survey (Figure 6.4). Three companions were detected in this survey, but none of them were sub-stellar (<80 $M_{\rm Jup}$). Thus, the probability of detecting 0 companions for each model is given in Table 6.4.

Given these probabilities, our null result allows us to reject the A-type star model with a scaled up planet frequency for r_{cutoff} > 100 AU, with more than 95% confidence. This null result is also consistent with previous surveys that found that high mass planets at large orbital separations are rare (Nielsen et al. 2013; Biller et al. 2013; Desidera et al. 2015; Chauvin et al. 2015), noting that our simulations include both the planetary-mass companions as well as extrapolation of the BD companion mass ratio distribution. Based on RV measurements of A

r_{cutoff}	P(0) [%] sun-like star planet frequency	P(0) [%] A-type star planet frequency
20 AU	57	51
30 AU	49	39
80 AU	15	5
100 AU	10	3

Table 6.4 Probability of a null result in our A and F main sequence star survey.

stars, Bowler et al. (2010) suggest positive values for the power law indexes of the mass and separation distributions, with high confidence. According to our Monte Carlo simulations, if we assume positive power law indexes, the probability of a null result is less than 0.1%, regardless of the planet frequency or the radius cutoff assumed. As suggested by Vigan et al. (2012), the inconsistency of direct imaging survey results with the distribution parameters from RV observations around A-stars (Bowler et al. 2010) suggests that different planet populations are probed by RV measurements at small separations than direct imaging at wide separations.

6.4 Comparison of the APP and Direct Imaging

There have been several other surveys focused on searching for planets around A stars (SEEDS: Janson et al. 2013; Brandt et al. 2014, NICI: Biller et al. 2013; Nielsen et al. 2013; Wahhaj et al. 2013, IDPS: Vigan et al. 2012, NACO Large Survey: Desidera et al. 2015; Chauvin et al. 2015, L'-band NACO: Rameau et al. 2013a). Our results are most comparable to Rameau et al. (2013a) since data were taken in L'-band. These surveys have detected low-mass stellar companions (Rameau et al. 2013a; Vigan et al. 2012), and brown dwarfs (Nielsen et al. 2013; Brandt et al. 2014). Our survey of only 13 targets yielded three low-mass companions. The dark 180° hole due to the APP is expected to increase sensitivity over direct imaging from 0.″2 to 0.″7. Without non-coronagraphic data of all of these targets, it is challenging to determine which benefited from the APP. However, four of our targets were also directly imaged in L'-band by Rameau et al. (2013a), allowing direct comparison of the sensitivity (Figure 6.5). We accessed the archival raw direct imaging data, processed it with PCA and follow the strategy detailed in Section 6.2.2 to ensure the data are reduced identically to the APP data.

These data are not ideal for comparison as they have different integration times, field rotation, and airmass. However, we compare the contrast curves for the two datasets for each target (Figure 6.5). HD 12894 and HD 102647 show increased sensitivity due to the APP. These targets show the expected decrease in sensitivity around 0.″8, where the PSF matches direct imaging (the "outside" of the dark hole). Beyond this angular separation, direct imaging performs slightly better than the APP, as expected (Kenworthy et al. 2010). The HD 984 contrast curves are nearly identical for direct imaging and the APP. Direct imaging performs better for HD 25457. This target does not achieve an increase in sensitivity from the APP at smaller radii, as was expected.

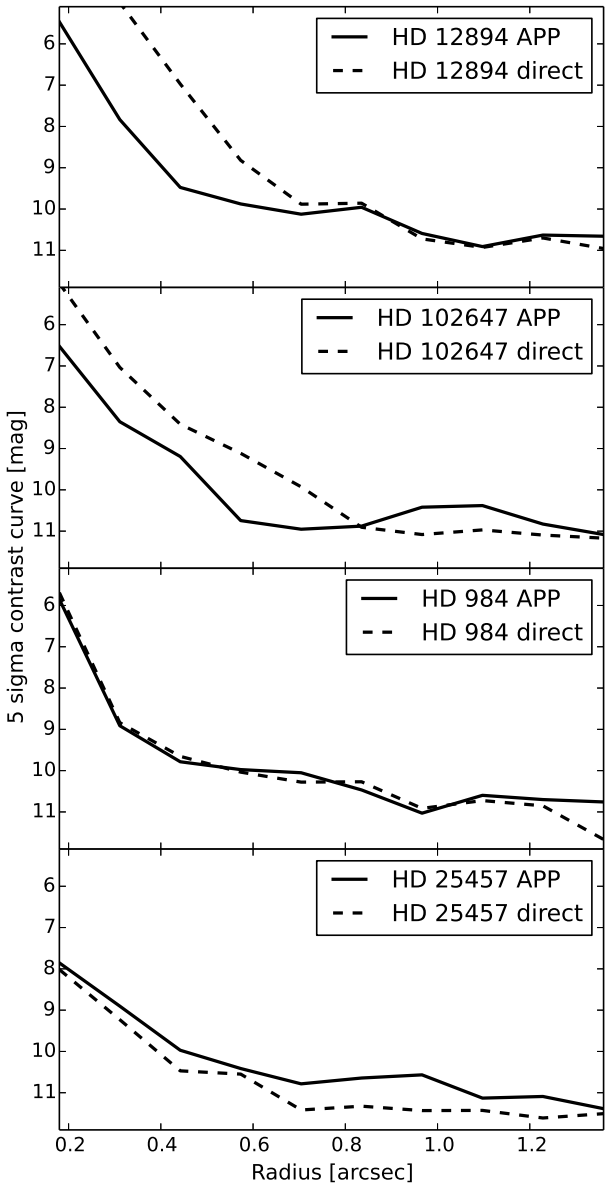

Figure 6.5 5σ contrast curves for the four targets which overlap with the direct imaging targets in Rameau et al. (2013a). HD 12894 and HD 102647 benefited from the use of the APP over direct imaging, seen by the "bump" in the contrast curve at $\sim 0\farcs7$. The bump shows that the APP suppressed diffraction more effectively than direct imaging would have under similar conditions. The curves are scaled so each target is the same integration time.

It is challenging to draw conclusions from these four datasets alone, as the rotation angle, seeing conditions, and integration times are not identical. However, in two of the four cases, the APP is more sensitive than direct imaging at small angular separations. At best, the APP provides 1-2 mag increased sensitivity from 0.″2 to 0.″8. Achieving better detection limits at smaller inner working angles is necessary to reach closer-in planets (Chauvin et al. 2010; Lafrenière et al. 2007; Nielsen & Close 2010). The APP, like all coronagraphs, is condition sensitive. These results suggest that a larger sample size with controlled data conditions should be performed to assess when the APP coronagraph outperforms direct imaging.

6.5 Conclusion

We present the results from a survey of carefully selected A- and F-type main sequence stars, searching for exoplanet companions. We aim to put direct imaging constraints on the occurrence of sub-stellar companions as a function of stellar mass. We obtained data on thirteen nearby (d<65 pc), young (<125 Myr) targets with the APP coronagraph on NACO/VLT. We are sensitive to planet masses (2 to 10 M_{Jup}) on Solar System scales (≤30 AU) for all but one of our targets. We detected a new M6.0 ± 0.5 dwarf companion to HD 984 and confirm stellar companions to HD 12894 and HD 20385, discovered shortly after our survey data were acquired. Our photometry and astrometry for these companions are consistent with the values reported at the time of their discovery (Biller et al. 2013; Hartkopf et al. 2012). We found zero false positives in our L'-band data, as all of our detected point sources were bona-fide companions. We perform Monte Carlo simulations to determine the expected probability of detecting low-mass companions in our survey, based on our sensitivity and assumed semi-major axis distributions. Our non-detection of substellar companions ($< 80\,M_{Jup}$) allows us to rule out the A-star frequency model distribution for >100 AU, with 95% confidence. We compare our APP coronagraphic data sensitivity with archival non-coronagraphic data for four targets and comment on when the performance is improved. We suggest a dedicated comparison survey is necessary to determine the appropriate targets and observing conditions when the APP coronagraph will consistently outperform direct imaging.

Acknowledgments

TM and MAK acknowledge funding under the Marie Curie International Reintegration Grant 277116 submitted under the Call FP7-PEOPLE-2010-RG. Part of this work has been carried out within the frame of the National Centre for Competence in Research PlanetS supported by the Swiss National Science Foundation. SPQ and MRM acknowledge the financial support of the SNSF. EEM acknowledges support from NSF award AST-1313029. This paper makes use of the SIMBAD Database and the Vizier Online Data Catalog.

References

Alibert Y., Mordasini C., Benz W., 2011, A&A, 526, A63
Amara A., Quanz S. P., 2012, MNRAS, 427, 948
Bailey V., Hinz P. M., Currie T., Su K. Y. L., Esposito S., Hill J. M., Hoffmann W. F., Jones T., Kim J., Leisenring J., Meyer M., Murray-Clay R., Nelson M. J., Pinna E., Puglisi A., Rieke G., Rodigas T., Skemer A., Skrutskie M. F., Vaitheeswaran V., Wilson J. C., 2013, ApJ, 767, 31
Bailey V., Meshkat T., Reiter M., Morzinski K., Males J., Su K. Y. L., Hinz P. M., Kenworthy M., Stark D., Mamajek E., Briguglio R., Close L. M., Follette K. B., Puglisi A., Rodigas T., Weinberger A. J., Xompero M., 2014, ApJL, 780, L4
Baraffe I., Chabrier G., Barman T. S., Allard F., Hauschildt P. H., 2003, A&A, 402, 701
Barenfeld S. A., Bubar E. J., Mamajek E. E., Young P. A., 2013, ApJ, 766, 6
Biller B. A., Liu M. C., Wahhaj Z., Nielsen E. L., Hayward T. L., Males J. R., Skemer A., Close L. M., Chun M., Ftaclas C., Clarke F., Thatte N., Shkolnik E. L., Reid I. N., Hartung M., Boss A., Lin D., Alencar S. H. P., de Gouveia Dal Pino E., Gregorio-Hetem J., Toomey D., 2013, ApJ, 777, 160
Bowler B. P., Johnson J. A., Marcy G. W., Henry G. W., Peek K. M. G., Fischer D. A., Clubb K. I., Liu M. C., Reffert S., Schwab C., Lowe T. B., 2010, ApJ, 709, 396
Brandt T. D., McElwain M. W., Turner E. L., Mede K., Spiegel D. S., Kuzuhara M., Schlieder J. E., Wisniewski J. P., Abe L., Biller B., Brandner W., Carson J., Currie T., Egner S., Feldt M., Golota T., Goto M., Grady C. A., Guyon O., Hashimoto J., Hayano Y., Hayashi M., Hayashi S., Henning T., Hodapp K. W., Inutsuka S., Ishii M., Iye M., Janson M., Kandori R., Knapp G. R., Kudo T., Kusakabe N., Kwon J., Matsuo T., Miyama S., Morino J.-I., Moro-Martín A., Nishimura T., Pyo T.-S., Serabyn E., Suto H., Suzuki R., Takami M., Takato N., Terada H., Thalmann C., Tomono D., Watanabe M., Yamada T., Takami H., Usuda T., Tamura M., 2014, ApJ, 794, 159
Casagrande L., Schönrich R., Asplund M., Cassisi S., Ramírez I., Meléndez J., Bensby T., Feltzing S., 2011, A&A, 530, A138
Chauvin G., Lagrange A.-M., Bonavita M., Zuckerman B., Dumas C., Bessell M. S., Beuzit J.-L., Bonnefoy M., Desidera S., Farihi J., Lowrance P., Mouillet D., Song I., 2010, A&A, 509, A52
Chauvin G., Vigan A., Bonnefoy M., Desidera S., Bonavita M., Mesa D., Boccaletti A., Buenzli E., Carson J., Delorme P., Hagelberg J., Montagnier G., Mordasini C., Quanz S. P., Segransan D., Thalmann C., Beuzit J.-L., Biller B., Covino E., Feldt M., Girard J., Gratton R., Henning T., Kasper M., Lagrange A.-M., Messina S., Meyer M., Mouillet D., Moutou C., Reggiani M., Schlieder J. E., Zurlo A., 2015, A&A, 573, A127
Chen C. H., Mittal T., Kuchner M., Forrest W. J., Lisse C. M., Manoj P., Sargent B. A., Watson D. M., 2014, ApJS, 211, 25
Clanton C., Gaudi B. S., 2014, ApJ, 791, 90
Cox A. N., 2000, Allen's astrophysical quantities

Crepp J. R., Johnson J. A., 2011, ApJ, 733, 126
Cumming A., Butler R. P., Marcy G. W., Vogt S. S., Wright J. T., Fischer D. A., 2008, PASP, 120, 531
Cutri R. M., Skrutskie M. F., van Dyk S., Beichman C. A., Carpenter J. M., Chester T., Cambresy L., Evans T., Fowler J., Gizis J., Howard E., Huchra J., Jarrett T., Kopan E. L., Kirkpatrick J. D., Light R. M., Marsh K. A., McCallon H., Schneider S., Stiening R., Sykes M., Weinberg M., Wheaton W. A., Wheelock S., Zacarias N., 2003, VizieR Online Data Catalog, 2246, 0
De Rosa R. J., Patience J., Wilson P. A., Schneider A., Wiktorowicz S. J., Vigan A., Marois C., Song I., Macintosh B., Graham J. R., Doyon R., Bessell M. S., Thomas S., Lai O., 2014, MNRAS, 437, 1216
Desidera S., Covino E., Messina S., Carson J., Hagelberg J., Schlieder J. E., Biazzo K., Alcalá J. M., Chauvin G., Vigan A., Beuzit J. L., Bonavita M., Bonnefoy M., Delorme P., D'Orazi V., Esposito M., Feldt M., Girardi L., Gratton R., Henning T., Lagrange A. M., Lanzafame A. C., Launhardt R., Marmier M., Melo C., Meyer M., Mouillet D., Moutou C., Segransan D., Udry S., Zaidi C. M., 2015, A&A, 573, A126
Fischer D. A., Valenti J., 2005, ApJ, 622, 1102
Hartkopf W. I., Tokovinin A., Mason B. D., 2012, AJ, 143, 42
Heinze A. N., Hinz P. M., Sivanandam S., Kenworthy M., Meyer M., Miller D., 2010, ApJ, 714, 1551
Hinkley S., Oppenheimer B. R., Soummer R., Brenner D., Graham J. R., Perrin M. D., Sivaramakrishnan A., Lloyd J. P., Roberts Jr. L. C., Kuhn J., 2009, ApJ, 701, 804
Janson M., Brandt T. D., Moro-Martín A., Usuda T., Thalmann C., Carson J. C., Goto M., Currie T., McElwain M. W., Itoh Y., Fukagawa M., Crepp J., Kuzuhara M., Hashimoto J., Kudo T., Kusakabe N., Abe L., Brandner W., Egner S., Feldt M., Grady C. A., Guyon O., Hayano Y., Hayashi M., Hayashi S., Henning T., Hodapp K. W., Ishii M., Iye M., Kandori R., Knapp G. R., Kwon J., Matsuo T., Miyama S., Morino J.-I., Nishimura T., Pyo T.-S., Serabyn E., Suenaga T., Suto H., Suzuki R., Takahashi Y., Takami M., Takato N., Terada H., Tomono D., Turner E. L., Watanabe M., Wisniewski J., Yamada T., Takami H., Tamura M., 2013, ApJ, 773, 73
Johnson J. A., Aller K. M., Howard A. W., Crepp J. R., 2010, PASP, 122, 905
Johnson J. A., Butler R. P., Marcy G. W., Fischer D. A., Vogt S. S., Wright J. T., Peek K. M. G., 2007, ApJ, 670, 833
Jurić M., Tremaine S., 2008, ApJ, 686, 603
Kasper M., Apai D., Janson M., Brandner W., 2007, A&A, 472, 321
Kenworthy M., Quanz S., Meyer M., Kasper M., Girard J., Lenzen R., Codona J., Hinz P., 2010, The Messenger, 141, 2
Kenworthy M. A., Meshkat T., Quanz S. P., Girard J. H., Meyer M. R., Kasper M., 2013, ApJ, 764, 7
Kraus A. L., Shkolnik E. L., Allers K. N., Liu M. C., 2014, AJ, 147, 146
Lafrenière D., Doyon R., Marois C., Nadeau D., Oppenheimer B. R., Roche P. F., Rigaut F., Graham J. R., Jayawardhana R., Johnstone D., Kalas P. G., Macintosh B., Racine R., 2007, ApJ, 670, 1367

Lagrange A.-M., Bonnefoy M., Chauvin G., Apai D., Ehrenreich D., Boccaletti A., Gratadour D., Rouan D., Mouillet D., Lacour S., Kasper M., 2010, Science, 329, 57
Lagrange A.-M., Gratadour D., Chauvin G., Fusco T., Ehrenreich D., Mouillet D., Rousset G., Rouan D., Allard F., Gendron É., Charton J., Mugnier L., Rabou P., Montri J., Lacombe F., 2009, A&A, 493, L21
Lenzen R., Hartung M., Brandner W., Finger G., Hubin N. N., Lacombe F., Lagrange A.-M., Lehnert M. D., Moorwood A. F. M., Mouillet D., 2003, in Society of Photo-Optical Instrumentation Engineers (SPIE) Conference Series, Vol. 4841, Society of Photo-Optical Instrumentation Engineers (SPIE) Conference Series, Iye M., Moorwood A. F. M., eds., pp. 944–952
Luhman K. L., Stauffer J. R., Mamajek E. E., 2005, ApJL, 628, L69
Mamajek E. E., Bell C. P. M., 2014, MNRAS, 445, 2169
Marois C., Lafrenière D., Doyon R., Macintosh B., Nadeau D., 2006, ApJ, 641, 556
Marois C., Macintosh B., Barman T., Zuckerman B., Song I., Patience J., Lafrenière D., Doyon R., 2008, Science, 322, 1348
Marois C., Macintosh B., Véran J.-P., 2010, in Society of Photo-Optical Instrumentation Engineers (SPIE) Conference Series, Vol. 7736, Society of Photo-Optical Instrumentation Engineers (SPIE) Conference Series
Mason B. D., Wycoff G. L., Hartkopf W. I., Douglass G. G., Worley C. E., 2011, VizieR Online Data Catalog, 1, 2026
Meshkat T., Bailey V. P., Su K. Y. L., Kenworthy M. A., Mamajek E. E., Hinz P. M., Smith P. S., 2015, ApJ, 800, 5
Meshkat T., Kenworthy M. A., Quanz S. P., Amara A., 2014, ApJ, 780, 17
Nielsen E. L., Close L. M., 2010, ApJ, 717, 878
Nielsen E. L., Liu M. C., Wahhaj Z., Biller B. A., Hayward T. L., Close L. M., Males J. R., Skemer A. J., Chun M., Ftaclas C., Alencar S. H. P., Artymowicz P., Boss A., Clarke F., de Gouveia Dal Pino E., Gregorio-Hetem J., Hartung M., Ida S., Kuchner M., Lin D. N. C., Reid I. N., Shkolnik E. L., Tecza M., Thatte N., Toomey D. W., 2013, ApJ, 776, 4
Pourbaix D., Tokovinin A. A., Batten A. H., Fekel F. C., Hartkopf W. I., Levato H., Morell N. I., Torres G., Udry S., 2009, VizieR Online Data Catalog, 1, 2020
Quanz S. P., Amara A., Meyer M. R., Kenworthy M. A., Kasper M., Girard J. H., 2013, ApJL, 766, L1
Quanz S. P., Lafrenière D., Meyer M. R., Reggiani M. M., Buenzli E., 2012, A&A, 541, A133
Quanz S. P., Meyer M. R., Kenworthy M. A., Girard J. H. V., Kasper M., Lagrange A.-M., Apai D., Boccaletti A., Bonnefoy M., Chauvin G., Hinz P. M., Lenzen R., 2010, ApJL, 722, L49
Quanz S. P., Schmid H. M., Geissler K., Meyer M. R., Henning T., Brandner W., Wolf S., 2011, ApJ, 738, 23
Rameau J., Chauvin G., Lagrange A.-M., Boccaletti A., Quanz S. P., Bonnefoy M., Girard J. H., Delorme P., Desidera S., Klahr H., Mordasini C., Dumas C., Bonavita M., 2013a, ApJL, 772, L15
Rameau J., Chauvin G., Lagrange A.-M., Klahr H., Bonnefoy M., Mordasini C.,

Bonavita M., Desidera S., Dumas C., Girard J. H., 2013b, A&A, 553, A60
Rameau J., Chauvin G., Lagrange A.-M., Meshkat T., Boccaletti A., Quanz S. P., Currie T., Mawet D., Girard J. H., Bonnefoy M., Kenworthy M., 2013c, ApJL, 779, L26
Reggiani M., Meyer M. R., 2013, A&A, 553, A124
Rousset G., Lacombe F., Puget P., Hubin N. N., Gendron E., Fusco T., Arsenault R., Charton J., Feautrier P., Gigan P., Kern P. Y., Lagrange A.-M., Madec P.-Y., Mouillet D., Rabaud D., Rabou P., Stadler E., Zins G., 2003, in Society of Photo-Optical Instrumentation Engineers (SPIE) Conference Series, Vol. 4839, Society of Photo-Optical Instrumentation Engineers (SPIE) Conference Series, Wizinowich P. L., Bonaccini D., eds., pp. 140–149
Santos N. C., Israelian G., Mayor M., 2004, A&A, 415, 1153
Spiegel D. S., Burrows A., 2012, ApJ, 745, 174
van Leeuwen F., 2007, A&A, 474, 653
Vigan A., Patience J., Marois C., Bonavita M., De Rosa R. J., Macintosh B., Song I., Doyon R., Zuckerman B., Lafrenière D., Barman T., 2012, A&A, 544, A9
Wahhaj Z., Liu M. C., Nielsen E. L., Biller B. A., Hayward T. L., Close L. M., Males J. R., Skemer A., Ftaclas C., Chun M., Thatte N., Tecza M., Shkolnik E. L., Kuchner M., Reid I. N., de Gouveia Dal Pino E. M., Alencar S. H. P., Gregorio-Hetem J., Boss A., Lin D. N. C., Toomey D. W., 2013, ApJ, 773, 179